2482 J. Med. Chem. 2010, 53, 2482–2493
DOI: 10.1021/jm901645u

Journal of Medicinal Chemistry Article

Salicylic Acid Based Small Molecule Inhibitor for the Oncogenic Src Homology-2 Domain Containing Protein Tyrosine Phosphatase-2 (SHP2)†

Xian Zhang,[‡,⊥] Yantao He,[‡] Sijiu Liu,[‡] Zhihong Yu,[‡] Zhong-Xing Jiang,[‡] Zhenyun Yang,[§] Yuanshu Dong,[‡] Sarah C. Nabinger,[§] Li Wu,[‡,∥] Andrea M. Gunawan,[∥] Lina Wang,[‡] Rebecca J. Chan,[§] and Zhong-Yin Zhang*[,‡,∥]

[‡]*Department of Biochemistry and Molecular Biology,* [§]*Herman B. Wells Center for Pediatric Research, and* [∥]*Chemical Genomics Core Facility, Indiana University School of Medicine, 635 Barnhill Drive, Indianapolis, Indiana 46202, and* [⊥]*Center for Chemical Genetics and Drug Discovery and College of Chemistry, Nankai University, Tianjin, China*

Received November 6, 2009

The Src homology-2 domain containing protein tyrosine phosphatase-2 (SHP2) plays a pivotal role in growth factor and cytokine signaling. Gain-of-function SHP2 mutations are associated with Noonan syndrome, various kinds of leukemias, and solid tumors. Thus, there is considerable interest in SHP2 as a potential target for anticancer and antileukemia therapy. We report a salicylic acid based combinatorial library approach aimed at binding both active site and unique nearby subpockets for enhanced affinity and selectivity. Screening of the library led to the identification of a SHP2 inhibitor II-B08 (compound **9**) with highly efficacious cellular activity. Compound **9** blocks growth factor stimulated ERK1/2 activation and hematopoietic progenitor proliferation, providing supporting evidence that chemical inhibition of SHP2 may be therapeutically useful for anticancer and antileukemia treatment. X-ray crystallographic analysis of the structure of SHP2 in complex with **9** reveals molecular determinants that can be exploited for the acquisition of more potent and selective SHP2 inhibitors.

Introduction

Reversible tyrosine phosphorylation, catalyzed by the coordinated actions of protein tyrosine kinases (PTKs[a]) and protein tyrosine phosphatases (PTPs), is of critical importance to the regulation of signaling events that underlie virtually all essential cellular processes.[1,2] Not surprisingly, disturbance of the normal balance between PTK and PTP activity results in aberrant tyrosine phosphorylation, which has been linked to the etiology of several human diseases, including cancer.[3,4] For example, abnormal expression and activation of many PTKs, such as epidermal growth factor receptor and proto-oncogene products Src and Abl, are causative factors for a number of malignancies.[5] By catalyzing the removal of the phosphoryl group from tyrosine residues, the PTPs are generally viewed as negative regulators due to their ability to reverse the actions of PTKs, which usually drive signaling cascades. However, mounting genetic and biochemical evidence suggests that some PTPs can potentiate, rather than antagonize, signaling mediated by the PTKs. This mode of synergy enhances mitogenic processes, leading to cell transformation.

The Src homology-2 domain containing protein tyrosine phosphatase-2, SHP2, is a positive transducer of growth factor, cytokine, integrin, and hormone signaling pathways regulating processes such as cell proliferation, differentiation, adhesion, migration, and apoptosis.[6,7] In nearly all cases, the catalytic activity of SHP2 is required for full activation of the Ras-ERK1/2 cascade that is mediated through dephosphorylation of substrates that are negatively regulated by tyrosine phosphorylation.[6−8] The critical role of SHP2 in cell physiology is further underscored by the identification of mutations within SHP2, which are linked to several human diseases. Thus, germline mutations in SHP2 that cause hyperactivation of its phosphatase activity are associated with 50% Noonan syndrome, an autosomal dominant disorder that is estimated to occur in 1:1000 to 1:2500 live births in the U.S. and worldwide.[9,10] Many Noonan syndrome patients display hematologic abnormalities, including myeloid disorders and juvenile myelomonocytic leukemia (JMML).[10] Somatic gain-of-function mutations in SHP2 occur in 35% of individuals with JMML, as well as in acute myeloid leukemia (AML, 4%), myelodysplastic syndrome (10%), and acute lymphoid leukemia (7%).[11−15] In addition to childhood leukemia, SHP2 mutations also occur in adult AML (6%) as well as in solid tumors including lung adenocarcinoma, colon cancer, neuroblastoma, melanoma, and hepatocellular carcinoma.[16−18] Finally, SHP2 is also implicated in gastric ulcer and, ultimately, gastric carcinoma caused by *Helicobacter pylori*, which harbors a key virulence factor CagA that promotes SHP2 activation when it is tyrosine phosphorylated by the host Src family kinases.[19] Collectively, these genetic and biochemical observations identify SHP2 as the first bona fide oncogene in the PTP superfamily.

In view of the importance of SHP2 in various kinds of leukemias and solid tumors, SHP2 represents an exciting

†The coordinates for the structure of the SHP2·II-B08 (compound **9**) complex (accession number 3JRL) have been deposited in the Protein Data Bank.

*To whom correspondence should be addressed. Phone: 317-274-8025. Fax: 317-274-4686. E-mail: zyzhang@iupui.edu.

[a]Abbreviations: SHP2, Src homology-2 domain containing protein tyrosine phosphatase-2; PTP, protein tyrosine phosphatase; PTK, protein tyrosine kinase; ERK, extracellular signal-regulated protein kinase; EGF, epidermal growth factor; GM-CSF, granulocyte macrophage colony stimulating factor.

 Published on Web 02/19/2010

target for anticancer and antileukemia therapy. Moreover, given the obligatory requirement of SHP2 function in multiple oncogenic receptor tyrosine kinase pathways, inhibition of SHP2 may also prove effective for cancers with coactivation of receptor PTKs, which respond poorly to kinase inhibitor monotherapy.[20] Understandably, there is increasing interest in targeting SHP2 for therapeutic development.[21−25] However, obtaining SHP2 inhibitors with optimal potency and pharmacological properties has been difficult primarily because of the highly conserved and positively charged nature of the active site pocket shared by all PTP family members. We describe here a salicylic acid based combinatorial library approach that led to the identification of a SHP2 inhibitor II-B08 (compound **9**) with highly efficacious cellular activity. This proof-of-principle SHP2 inhibitor blocks growth factor stimulated ERK1/2 activation and hematopoietic progenitor proliferation, validating the concept that chemical inhibition of SHP2 may be therapeutically useful for anticancer and antileukemia treatment. X-ray crystallographic analysis of compound **9**-bound SHP2 structure together with structure and activity studies reveal molecular determinants that can be exploited for the acquisition of more potent and selective SHP2 inhibitors.

Results and Discussion

Identification of Compound 9 as a SHP2 Inhibitor from a Salicylic Acid Based Combinatorial Library. As discussed above, SHP2 is an outstanding target for oncology. However, the common architecture of the active site (i.e., pTyr-binding pocket) shared by all PTPs poses a significant problem for the acquisition of selective SHP2 inhibitors. Fortunately, it has been recognized that pTyr alone is not sufficient for high-affinity binding and residues flanking pTyr are important for PTP substrate recognition.[26] These findings point to a conceptual framework for PTP inhibitor design, namely, bidentate ligands capable of engaging both the active site and an adjacent less-conserved subpocket for enhanced affinity and selectivity. In principle, active site-directed, potent, and selective PTP inhibitors can be devised by tethering a nonhydrolyzable pTyr mimetic to appropriately functionalized moieties to bind both the active site and a unique nearby subpocket.[26,27] Indeed, a number of potent and selective PTP1B inhibitors have been developed using this strategy.[28]

Unfortunately, the highly positively charged pTyr-binding pocket impedes the development of inhibitors with favorable bioavailability. Most of the pTyr mimetics described in the literature are not druglike and thus are deficient in cell membrane permeability. Indeed, the lack of cellular efficacy of existing PTP inhibitors represents a major obstacle in developing phosphatase-based therapeutics. Consequently, there is continued interest in developing pTyr mimetics with more acceptable physicochemical properties. We recently discovered from an in silico DOCK screening campaign that the natural product salicylic acid can serve as a pTyr mimetic.[29] We further demonstrated that naphthyl and polyaromatic salicylic acid derivatives exhibit enhanced affinity for PTPs relative to the corresponding single ring compounds.[29,30] Therefore, we sought to develop bicyclic salicylic acid based PTP inhibitors that carry sufficient polar and nonpolar interactions with the active site and yet possess improved pharmacological properties. Bioactive natural products are very promising starting points for drug development because they are evolutionarily selected and validated for interfering and interacting with biological targets. The indole nucleus is a prominent structural scaffold found in numerous natural products and synthetic compounds with vital medicinal value.[31,32] To this end, we have focused our attention on indole-based salicylic acids as PTP active-site-directed pTyr mimetics. We hypothesized that an indole-based salicylic acid may bind the active site and interact in the desired inhibitory fashion with the PTPs, and additional diversity elements to which the salicylic core is attached to should render the inhibitors PTP isozyme-selective.

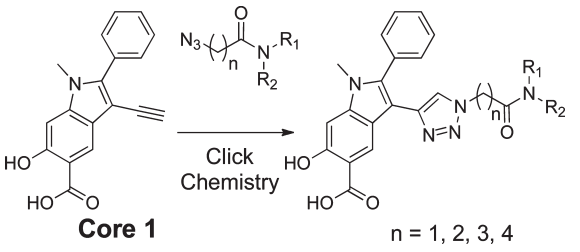

Figure 1. Strategy for the construction of an indole salicylic acid based library using click chemistry.

To target both the active site and an adjacent, peripheral secondary binding site in SHP2, we have developed a salicylic acid based combinatorial library approach that entails the following criteria: (1) each member will be of a modular, bidentate structure containing both an active-site-directed core (the salicylic acid derivative) and a diversity element for interaction with adjacent peripheral sites in SHP2; (2) both the core group and the diversity elements will possess favorable pharmacological properties; (3) each member will be efficiently assembled in situ for facile screening against SHP2. We chose click chemistry for library construction because it offers an expedient way to connect two components together with high yield and purity under extremely mild conditions.[33] More importantly, the click reaction can be conducted in aqueous solution in the absence of deleterious reagents, thus allowing direct screening and identification of hits from the library. In fact, click chemistry has found increasing applications in lead discovery and optimization for a number of enzymes including the PTPs.[34−39]

Figure 1 depicts a focused library-based strategy for the acquisition of potent and selective SHP2 inhibitory agents that are capable of bridging both the active site and an adjacent peripheral site. The library contains (a) a salicylic acid core to engage the PTP active site and (b) four alkyl linkers of one to four methylene units to tether the pTyr mimetic to (c) a structurally diverse set of amines and hydrazines aimed at capturing additional interactions with adjacent pockets surrounding the active site. In the interest of keeping the library to a reasonable size, we selected 53 amines and hydrazines that vary by molecular weight, charge, polarity, hydrophobicity, sterics, etc. and therefore provide a reasonable (albeit limited) structural diversity to increase the number and strength of noncovalent interactions between SHP2 and the inhibitor.

As shown in Scheme 1, the salicylic acid core **1** was synthesized in eight steps with Sonogashira coupling and an electrophilic cyclization as key steps. After esterification of 4-aminosalicylic acid with dimethyl sulfate, compound **2** was isolated in 86% yield which was then treated with paraformaldehyde and $NaCNBH_3$ to give the product *N*, *N*-dimethylaniline **3** with good yield. Selective iodination of

Scheme 1. Synthesis of the Alkyne-Containing Salicylic Acid Core **1**[a]

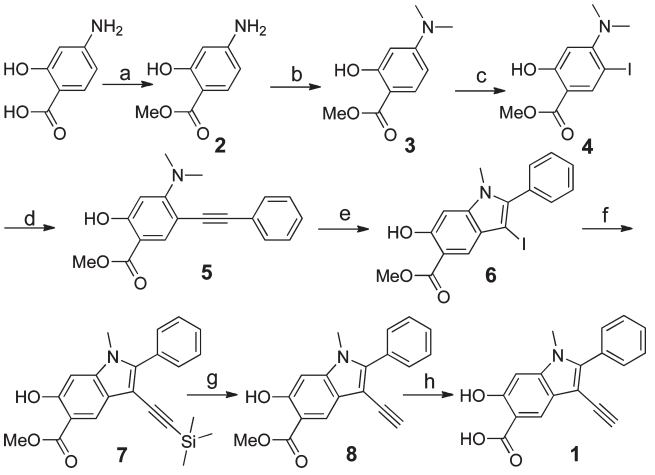

[a] Conditions: (a) Me_2SO_4, Na_2CO_3, acetone, room temp, 86%; (b) $(CH_2O)_n$, $NaCNBH_3$, AcOH, room temp, 78%; (c) I_2, K_2CO_3, water, room temp, 42%; (d) phenylacetylene, $Pd(PPh_3)_2Cl_2$, CuI, Et_3N, DMF, 89%; (e) I_2, CH_2Cl_2, room temp, 87%; (f) trimethylsilylacetylene, $Pd(PPh_3)_2Cl_2$, CuI, Et_3N, DMF, room temp, 73%; (g) TBAF, THF, room temp, 69%; (h) KOH, THF/H_2O, reflux, 38%.

compound **3** with iodine gave methyl 4-(dimethylamino)-2-hydroxy-5-iodobenzoate **4**, which was then coupled with the commercially available phenylacetene with Sonogashira coupling to afford compound **5** with excellent yield. Compound **6** was constructed by electrophilic cyclization of **5** with iodine in 89% yield. Key compound **7** was generated through another Pd(0)-catalyzed Sonogashira coupling of compound **6** with trimethylsilyacetylene. Finally, sequential removal of the protective groups in compound **7** with TBAF and KOH gave the salicylic acid core **1**.

To increase potency and selectivity, the strategically positioned alkyne in salicylic acid core **1** was tethered to 212 different azide-containing diversity elements (53 discrete amines and hydrazines (Figure 2) with four alkyl linkers of one to four methylenes length), using click chemistry or the Cu(I)-catalyzed [3 + 2] azide−alkyne cycloaddition reaction (Figure 1). The azide-containing building blocks were synthesized in a one-pot procedure (Scheme 2) in which amines or hydrazines were reacted with the acyl chloride linkers in *N*,*N*-dimethylformamide (DMF) followed by S_N2 reaction with sodium azide to generate the corresponding azides.

To construct the 212-member library, each azide (32 mM) was coupled with the alkyne containing core **1** (26.6 mM) in the presence of 1.33 mM $CuSO_4$ and 6.64 mM sodium ascorbate and 0.798 mM TBTA (tris(benzyltriazolylmethyl)-amine) in 0.5 mL solvent ($THF/t\text{-}BuOH/H_2O$ = 1:1:1) at room temperature for 12 h. The products were assessed by LC−MS and used directly for screening without further purification (the purity was in the range 40−70%).

The ability of the library compounds to inhibit the SHP2-catalyzed hydrolysis of *p*-nitrophenyl phosphate (*p*NPP) was assessed at pH 7 and 25 °C. Out of the 212-member library, 5 compounds displayed measurable inhibitory activity at ~10 μM. Resynthesis of the hits confirmed that they were genuine inhibitors for SHP2 with IC_{50} values in the low micromolar range (Table 1). These values compare very favorable to the alkyne-containing salicylic acid core, which displays an IC_{50} of 212 ± 23 μM for SHP2. The results

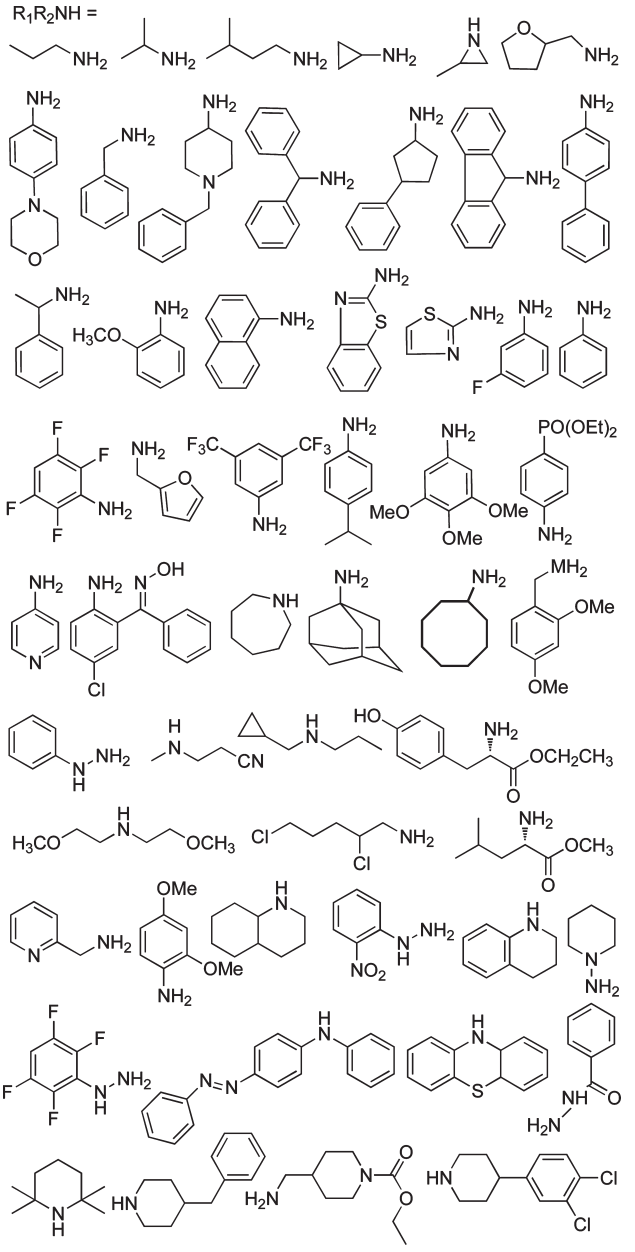

Figure 2. Chemical structures of 53 amines and hydrazines.

Scheme 2. Synthesis of Azide-Tagged Diversity Elements

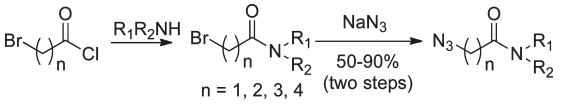

indicate that the linker and amine diversity element contribute significantly to SHP2 binding. In addition, the structure and activity data revealed that compounds with substituted biphenyls as the diversity elements were preferentially selected by SHP2. Compound **9** (Table 1) appeared to be the most potent for SHP2 with an IC_{50} of 5.5 ± 0.4 μM and was selected for further characterization. Kinetic analysis indicated that **9** is a reversible and noncompetitive inhibitor for SHP2 with a K_i of 5.2 ± 0.3 μM (Figure 3). To determine the specificity for **9**, its inhibitory activity toward a panel of mammalian PTPs including cytosolic PTPs, SHP1, PTP1B, Lyp, HePTP, and FAP1, the receptor-like PTPs, CD45,

Table 1. IC_{50} Values (μM) of Top Hits for SHP2 Identified from the Library[a]

Compound	Structure	IC_{50} (μM)
II-B08 (**9**)	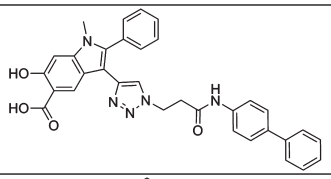	5.5 ± 0.4
II-A09 (**10**)	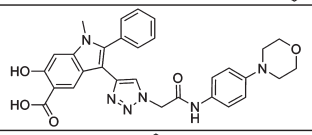	7.8 ± 0.8
II-A12 (**11**)	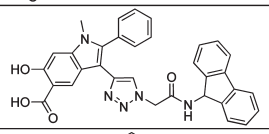	10.4 ± 0.6
II-A15 (**12**)	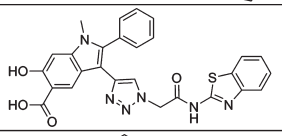	9.1 ± 0.4
II-D50 (**13**)	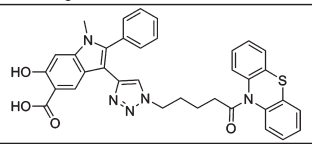	8 ± 1

[a] All measurements were made using *p*NPP as a substrate at pH 7.0, 25 °C, and $I = 0.15$ M.

LAR, and PTPα, the dual specificity phosphatases VHR, and Cdc14, and the low molecular weight PTP was measured. As shown in Table 2, compound **9** exhibits at least several-fold selectivity for SHP2 over all PTPs examined. Most importantly, compound **9** displays excellent cellular activity as shown below.

Cellular Activity of Compound 9. Our ultimate goal is to develop potent and specific SHP2 inhibitors as anticancer and antileukemia agents. Given the excellent potency and selectivity of **9** toward SHP2, we proceeded to evaluate its ability to inhibit SHP2-dependent signaling inside the cell. Previous studies have demonstrated that SHP2 promotes growth-factor-stimulated ERK1/2 activation and cell proliferation.[6,7] We have initially used human embryonic kidney 293 (HEK293) cells, as these cells are relatively easy to culture and express high levels of the EGF receptor, a pathway in which SHP2 is known to positively participate in.[40,41] Briefly, HEK293 cells were serum-deprived for 16 h followed by incubation with vehicle or 10 μM compound **9** for 3 h. Cells were then stimulated with EGF at 2 ng/mL for 5−60 min, total cellular lysates were resolved by SDS−PAGE, and levels of phospho-ERK1/2 were examined. As shown in Figure 4A, **9** strongly inhibits the sustained phase of ERK1/2 activation (60 min after EGF stimulation), which has been shown to depend on SHP2,[42] but not the initial transient phase (5−15 min), which is SHP2-independent and mediated by recruitment of growth factor receptor bound protein 2 (Grb2) and the Ras guanine nucleotide exchange factor Son of Sevenless (Sos).[43] Similar results were also obtained in NIH3T3 cells (data not shown). To investigate whether this inhibitory effect of **9** on SHP2-mediated signaling is dose-dependent, we pretreated HEK293 cells with 0−20 μM II-B08, followed by EGF stimulation for 60 min. Indeed, a concentration-dependent inhibition of the EGF-induced ERK1/2 activation by **9** was observed (Figure 4B). To ensure that the cellular activity displayed by **9** is not due to nonspecific effects, we also evaluated a structurally related but inactive II-B05 (compound **14**), which has an IC_{50} value

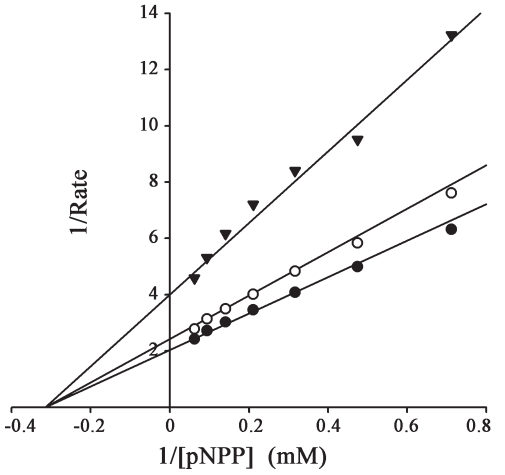

Figure 3. Lineweaver−Burk plot for compound **9**-mediated SHP2 inhibition. Compound **9** is a noncompetitive inhibitor of SHP2. Compound **9** concentrations were 0 (●), 1.0 (○), and 5.0 μM (▼), respectively.

Table 2. Selectivity of **9** against a Panel of PTPs[a]

PTP	IC_{50} (μM)
SHP2	5.5 ± 0.4
SHP1	15.7 ± 2.1
PTP1B	14.3 ± 1.5
HePTP	> 50
Lyp	25.0 ± 3.6
FAP1	20.3 ± 1.3
CD45	30.0 ± 6
LAR	> 50
PTPα	> 50
VHR	> 50
Cdc14A	> 50
LMWPTP	31.1 ± 1.9

[a] All measurements were made using *p*NPP as a substrate at pH 7.0, 25 °C, and $I = 0.15$ M.

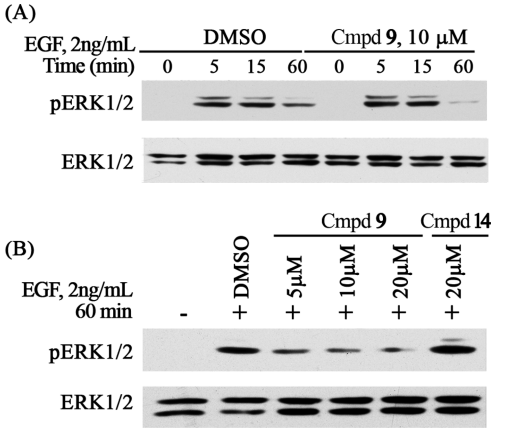

Figure 4. Compound **9** inhibits SHP2-dependent ERK1/2 activation: (A) immunoblot showing phospho-ERK1/2 levels from 0 to 60 min time points of EGF stimulation of HEK293 cells in the presence or absence of 10 μM compound **9**; (B) concentration dependence of inhibition of the EGF-induced sustained ERK1/2 activation by **9** in HEK293 cells.

Table 3. Crystallographic Data and Refinement Statistics for SHP2·**9** Complex

parameter	
space group	$P2_1$
cell dimensions	
a (Å)	39.5
b (Å)	75.8
c (Å)	48.2
β (deg)	98.5
data collection	
wavelength for data collection	0.97915
resolution (Å)	50.0−2.0
highest resolution shell (Å)	2.06−2.0
no. of unique reflections	18 718
completeness (%)	99.4 (99.1)[a]
redundancy	3.4
R_{merge}[b]	7.5 (30.8)[a]
$\langle I/\delta(I)\rangle$	13.7 (2.2)[a]
refinement	
resolution range (Å)	50−2.0
no. of reflections used ($F \geq 2.0\sigma(F)$)	18 673
no. of protein atoms	2075
no. of inhibitor	1
no. of water	142
R_{work}[c]/R_{free}[d]	19.1/25.1
rms deviations from ideal geometry	
bond length (Å)	0.006
bond angle (deg)	1.22
average *B* (Å^2)	31.7

[a] The value in parentheses corresponds to the highest resolution shell. [b] $R_{merge} = \sum_h\sum_i|I(h)_i - \langle I(h)\rangle|/\sum_h\sum_i I(h)_i$. [c] $R_{work} = \sum_h|F(h)_{calcd} - F(h)_{obsd}|/\sum_h F(h)_{obsd}$, where $F(h)_{calcd}$ and $F(h)_{obsd}$ were the refined calculated and observed structure factors, respectively. [d] R_{free} was calculated for a randomly selected 3.8% of the reflections that were omitted from refinement.

of 86 μM for SHP2 (Table 4). As expected, compound **14** at 20 μM elicits no appreciable change in pERK1/2 level when normalized by total ERK1/2 protein level (Figure 4B). The observation that **9** inhibits SHP2 in intact cells with similar potency as that toward isolated enzyme is remarkable, since previous PTP inhibitors have shown 100- to 10000-fold loss of potency from biochemical to cellular assays. Together, the data demonstrate that **9** is cell permeable and can effectively inhibit a major pathway positively regulated by SHP2.

As we observed inhibition of EGF-stimulated ERK1/2 activation in HEK293 cells, we next investigated whether **9** could inhibit gain-of-function SHP2 mutant-induced hematopoietic progenitor hyperproliferation in response to granulocyte macrophage colony stimulating factor (GM-CSF). Peripheral blood hematopoietic progenitors from JMML patients are hypersensitive to the cytokine GM-CSF.[44] Studies from our lab have demonstrated that somatic gain-of-function SHP2 mutations E76K, D61V, and D61Y induce hematopoietic progenitor hypersensitivity to GM-CSF.[45] On the basis of these findings, we predicted that hematopoietic progenitors expressing gain-of-function SHP2 mutants would display reduced proliferation in response to GM-CSF when treated with **9**. We compared the effect of 10 μM compound **9** on GM-CSF-stimulated hypersensitivity of wild-type SHP2, SHP2/E76K-, and SHP2/D61Y-expressing hematopoietic progenitors using [^{3}H]thymidine incorporation assays in response to increasing concentrations of GM-CSF. As previously found, expression of SHP2/E76K and SHP2/D61Y induced GM-CSF-stimulated hyperproliferation compared to cells expressing wild-type SHP2

Table 4. Structure and Activity for Compound **9**[a]

Compound	Structure	IC_{50} (μM)
Salicylic acid core **1**	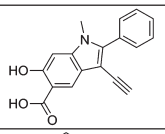	212 ± 23
II-A08 (**9a**)	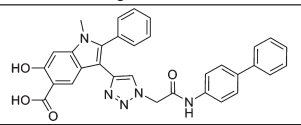	9.3 ± 0.5
9	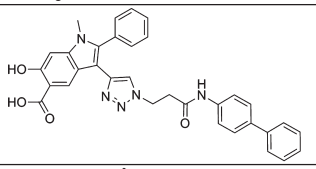	5.5 ± 0.4
II-C08 (**9b**)	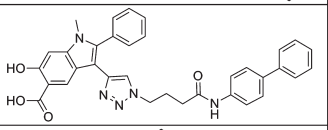	12 ± 1
II-B05 (**14**)	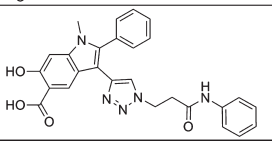	86 ± 3

[a] All measurements were made using *p*NPP as a substrate at pH 7.0, 25 °C, and I = 0.15 M.

(Figure 5). In the presence of 10 μM compound **9**, the hyperproliferation of mutant SHP2-expressing progenitors in response to GM-CSF was substantially reduced to levels similar to that observed with wild-type SHP2-expressing progenitors (Figure 5). These studies demonstrate that **9** is effective at significantly reducing GM-CSF-stimulated hyperproliferation induced by activating SHP2 mutations. Collectively, the results described above indicate that **9** is highly efficacious in cell-based assays and capable of blocking SHP2 activity inside the cell.

Molecular Basis of SHP2 Inhibition by Compound 9. To provide insight into the molecular basis for SHP2 inhibition by **9** and to aid the design of SHP2 inhibitors with improved potency and selectivity, we determined the crystal structure of the catalytic domain of SHP2 (residues 262−528) in complex with **9**. The SHP2·**9** complex crystallized in space group $P2_1$ with one molecule in the asymmetric unit. The crystals of the SHP2·**9** complex diffracted to 2.0 Å resolution, and the structure was solved by molecular replacement, using the apo-form of SHP2 catalytic domain (PDB accession 3B7O)[46] as the search model. The three-dimensional structure of SHP2·**9** was refined to a crystallographic *R*-factor of 19.1% (R_{free} = 25.1%), and the statistics for the data collection and refinement are shown in Table 3. The atomic model includes SHP2 residues 262−312 and 324−527 and all atoms of the inhibitor (Figure 6). Unambiguous electron densities are observed for all surface loops, including the PTP signature motif or the P-loop (residues 458−465) which harbors the active site nucleophile C459 and R465 for recognition of the phosphoryl moiety in the substrate), the pTyr recognition loop (residues 277−284) which confers specificity to pTyr, the WPD loop (residues 421−431) which contains the general acid−base catalyst D425, and the Q-loop (residues 501−507) which contains the conserved Q506 required to position and activate a water molecule for hydrolysis of the phosphoenzyme intermediate.[47]

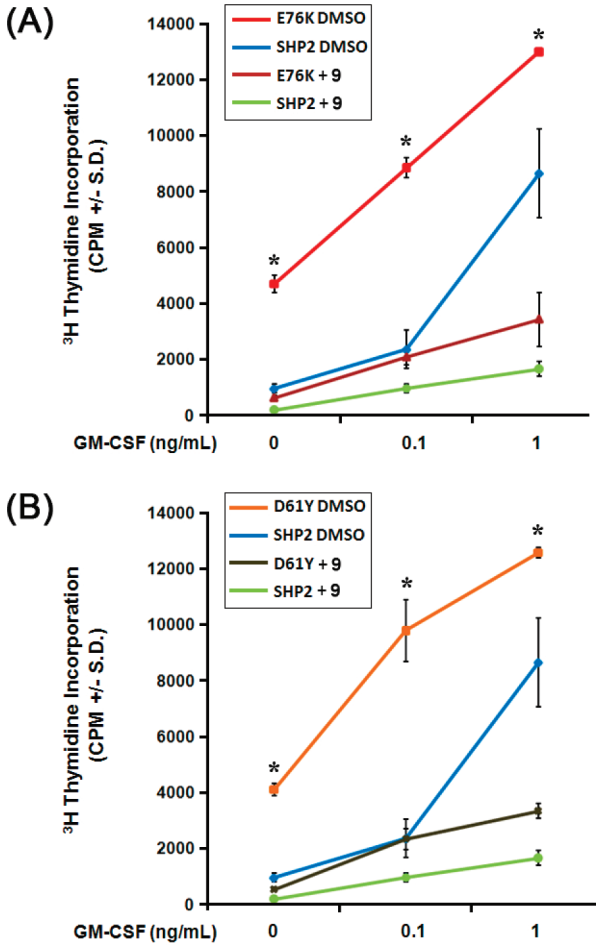

Figure 5. Compound **9** inhibits GM-CSF-stimulated bone marrow low density mononuclear cell proliferation. (A, B) Bone marrow low density mononuclear cells retrovirally transduced with wild-type SHP2, SHP2/D61Y, or SHP2/E76K were serum- and growth factor-deprived, stimulated with increasing concentrations of GM-CSF (0−1 ng/mL) in the presence or absence of 10 μM compound **9** and subjected to [^{3}H]thymidine incorporation to measure cellular proliferation: $n = 3$, (*) $p < 0.005$ for DMSO vs **9** for both SHP2/D61Y- and SHP2/E76K-expressing cells at all concentrations of GM-CSF.

The overall structure of SHP2·**9** is similar to the ligand-free SHP2 structure used for molecular replacement, with the root-mean-square-derivation (rmsd) for all α-carbon positions between the two being 0.5 Å. The major difference between the two structures is electron density in the SHP2 active site corresponding to **9**, which was confirmed by analyzing the $|F_o| - |F_c|$ difference map contoured at 3.0σ (Figure 6B). This represents the first three-dimensional structure of SHP2 in complex with a small molecule ligand. As expected, the salicylic acid moiety of **9** is found in the SHP2 active-site pocket and forms extensive interactions with residues in the P-loop, the pTyr recognition loop, and the WPD loop (Figure 7). Specifically, the phenolic oxygen atom O_1 within the salicylic acid core makes a hydrogen bond with the main chain amide of R465 in the P-loop; the carboxylate O_2 forms two polar interactions with the side chains of R465 and Q510, and O_3 contributes two H-bonds with the side chains of R465 and W423, respectively. Additionally, the salicylic acid moiety also engages in five more polar interactions with SHP2, mediated by two water molecules (W1 and W2) in the active site (Figure 7). Thus, O_3 also

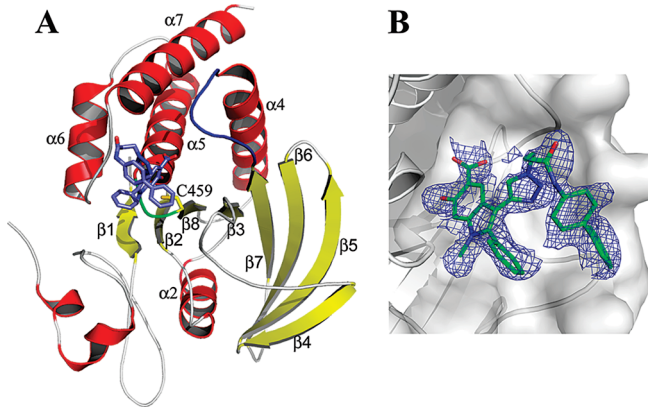

Figure 6. Crystal structure of SHP2 in complex with **9**. (A) Ribbon diagram of SHP2 catalytic domain in complex with inhibitor **9**. The molecule is oriented with the C-terminal end of the β_8 strand toward the viewer. α-Helices and β-strands are colored in red and yellow, respectively. The P-loop is shown in green and the WPD loop in blue. Compound **9** is shown in stick-and-bond mode. (B) $F_o - F_c$ difference map of SHP2 contoured at the 3.0σ level.

participates in a W2-mediated H-bond network with the backbone carbonyls of P424, D425, and G427 in the WPD loop whereas O_1 is hydrogen-bonded to W1, which makes a H-bond with the main chain amide of S460 in the P-loop and a polar interaction with the side chain of K366. In addition to these polar interactions, there are also van der Waals contacts between SHP2 and the salicylic acid core portion of **9**. For example, the indole ring of **9** interacts with the side chains of S460 and R465; the methyl group immediately attached to the indole ring has hydrophobic interactions with the side chains of Y279 and A461.

Although the salicylic acid core occupies the active site, the manner by which it interacts with SHP2 differs significantly from those observed between pTyr and PTP1B (Figure 8). Binding of pTyr or nonhydrolyzable pTyr mimetics to the PTPs usually accompanies the closure of the flexible WPD loop,[27,48,49] which harbors the catalytically essential general acid/base D425.[52] A strong stacking interaction between R465 in the P-loop and W423 of the WPD loop is found in the pTyr-bound PTP structures, which plays an important role in stabilizing the closed conformation. Interestingly, the WPD loop in SHP2 adopts an open conformation when **9** is bound. Compared to pTyr in PTP1B, the salicylic acid core moves ~3.5 Å toward the WPD loop (Figure 8). As a result, the carboxylate of the salicylic acid core makes direct polar contacts with the guanidinium group of R465 and the side chain of W423, precluding a favorable interaction between R465 and W423 to enable WPD loop closure. In addition, the W2-mediated interactions between O_3 and the backbone carbonyls of P424, D425, and G427 further prevent WPD loop closure. Molecular modeling suggests that substrate *p*NPP can still be accommodated by SHP2's active site in the presence of **9**. Since the WPD loop open conformation is catalytically incompetent, our structural observation that **9** binds SHP2 in the WPD loop open conformation is consistent with **9** being a noncompetitive inhibitor.

Further inspection of the structure of the SHP2·**9** complex revealed that, in addition to the salicylic acid core-dependent interactions, the distal phenyl ring P_4 in the biphenyl diversity element is sandwiched between the side chains of R362 and K364 in the β_5−β_6 loop (residues 362−365) (Figure 7). Interestingly, the β_5−β_6 loop is highly divergent among the

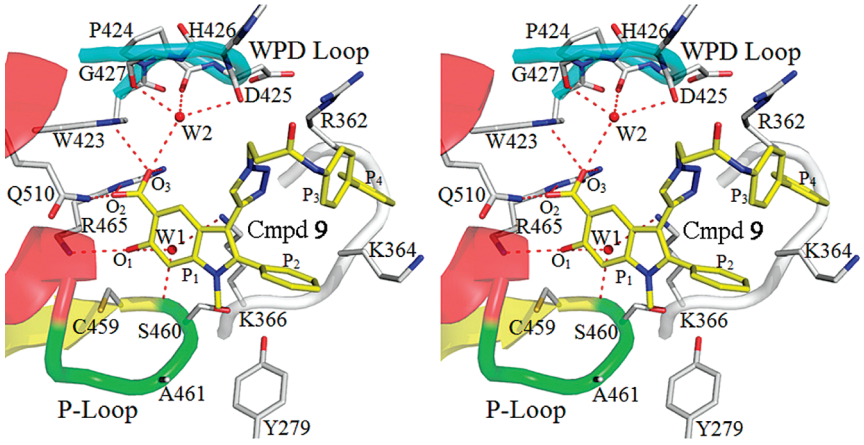

Figure 7. Detailed interactions between SHP2 and **9**. The P-loop and WPD loop are shown in green and blue, respectively. Atomic colors are as follows: oxygen, red; carbon, gray; sulfur, orange; nitrogen, blue. Ligand's carbon atoms are colored yellow. Polar interactions are highlighted with red dash lines.

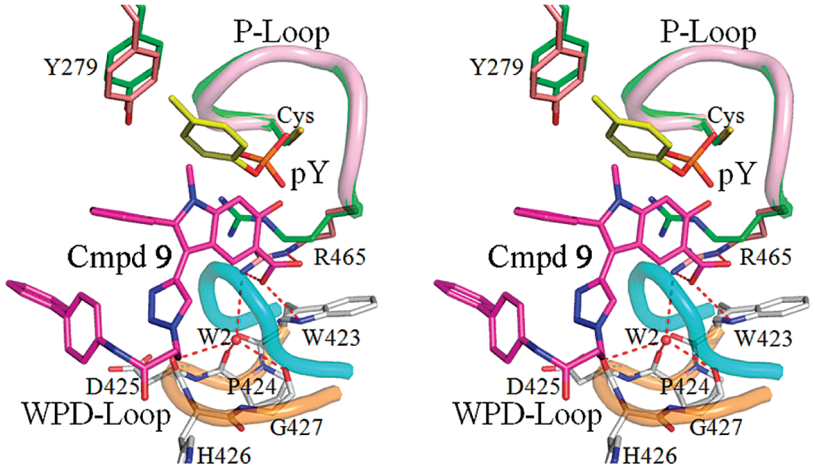

Figure 8. Superposition of SHP2·**9** and PTP1B·pY (PDB entry code 1EEN). The superposition was calculated with active site residues without the ligands. Active site of PTP1B is in the WPD loop closed conformation. pY is shown in yellow, the WPD loop is in blue, and the P-loop and other residues are in green. For the SHP2·**9** structure, the WPD loop is in the open conformation, with **9** shown in red, WPD loop in orange, the P-loop in green, Y279 and R465 in pink, and W423, P424, D425, H426, and G427 in gray.

PTPs (Figure 9) and has been implicated in substrate recognition by SHP1.[50] These additional nonpolar interactions between P_4 and residues R362 and K364 are likely responsible for the enhanced potency and selectivity of **9**. To directly show the involvement for these peripheral site interactions in SHP2 binding, we prepared and analyzed several compounds structurally related to **9** (Table 4). Consistent with the observed binding mode, **9** binds SHP2 with a 38.5-fold higher affinity than that of the salicylic acid core **1** alone (Table 4). Moreover, when the distal P_4 ring was removed from **9**, the IC_{50} value for the resulting compound **14** increased 15.6-fold. The importance of the interactions between P_4 and R362/K364 was further manifest by the observation that either a decrease or an increase in the linker size by one methylene unit led to a ~2-fold reduction in the IC_{50} values for II-A08 (**9a**) and II-C08 (**9b**), respectively (Table 4). These results are in excellent agreement with the structural observation, supporting the conclusion that interactions between P_4 and R362/K364 contribute to the enhanced potency of **9** for SHP2.

To determine whether the interactions between P_4 and R362/K364 also play a role in controlling compound **9** selectivity, we studied two SHP2 mutants bearing substitutions at residue K364, which corresponds to an Arg in SHP1 and a Ser in PTP1B (Figure 9). Substitutions at K364 are expected to perturb the interactions with the distal end of **9**. Kinetic analysis yielded an IC_{50} of 9.0 ± 0.3 μM for SHP2/K364R and of 10.8 ± 0.2 μM for SHP2/K364S. These IC_{50} values are 1.6- and 2.0-fold higher than that of wild-type SHP2, in accord with K364 playing a contributing role to compound **9** selectivity. They are also slightly lower than those determined for SHP1 and PTP1B, indicating that additional variable residues in SHP2 may also be involved in controlling compound **9** selectivity. Collectively, the structure and activity data plus results from mutational experiments are consistent with the structural observation that **9** achieves its potency and specificity by directly targeting regions that are structurally divergent in PTPs.

In summary, we describe here a salicylic acid based combinatorial library approach designed to target both the PTP active site and a unique nearby subpocket for enhanced affinity and selectivity. High throughput screening of the library led to the identification of a SHP2 inhibitor **9** with promising potency and selectivity. More importantly, **9** possesses highly efficacious cellular activity and is capable of blocking growth factor stimulated ERK1/2 activation as

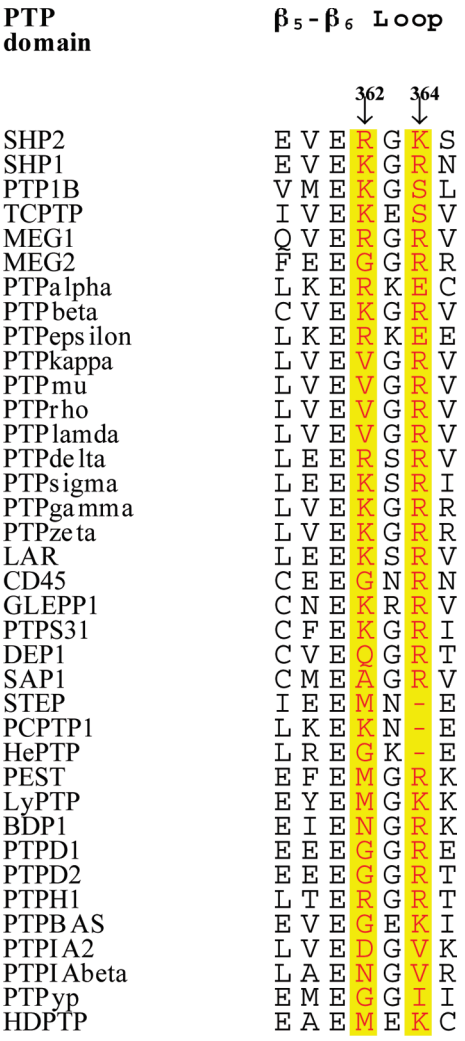

Figure 9. Amino acid sequence alignment of the $\beta_5-\beta_6$ loop among the PTPs.

well as blocking SHP2 gain-of-function mutant-induced hematopoietic progenitor hyperproliferation in response to GM-CSF. The results suggest that the bicyclic salicylic acid pharmacophore chemistry platform may provide a potential solution to overcome the bioavailability issue that has plagued the PTP drug discovery field for many years. X-ray crystallographic analysis of compound **9**-bound SHP2 structure reveals that the salicylic acid core occupies the PTP active site, while the distal biphenyl ring makes hydrophobic contacts with a region highly divergent among the PTPs. The atomic-level information on SHP2·**9** and studies of compound **9** derivatives and SHP2 mutants furnish a solid foundation for the design of more potent and selective SHP2-based small molecule therapeutics. Given the ease and versatility of the click chemistry based library construction methodology described in this report, it is expected that cell permeable, salicylic acid based small molecule inhibitors will become available for other PTPs as well.

Experimental Section

Materials and General Procedures. Polyethylene glycol (PEG3350) and buffers for crystallization were purchased from Hampton Research Co. *p*-Nitrophenyl phosphate (*p*NPP) was purchased from Fluke Co. Dithiothreitol (DTT) was provided by Fisher (Fair Lawn, NJ). For organic synthesis, reagents were used as purchased (Aldrich, Acros, Alfa Aesar, TCI) except where noted. ^{1}H and ^{13}C NMR spectra were obtained on a Bruker Avance II 500 MHz NMR spectrometer with TMS or residual solvent as standard. All column chromatography was performed using Dynamic Adsorbents 230−400 mesh silica gel (SiO_2) with the indicated solvent system unless otherwise noted. TLC analysis was performed using 254 nm glass-backed plates and visualized using UV light (254 nm). HPLC purification was carried out on a Waters Delta 600 equipped with a Sunfire Prep C_{18} OBD column (30 mm × 150 mm, 5 μm) with methanol−water (both containing 0.1% TFA) as mobile phase (gradient: 50−100% methanol, flow 10 mL/min). The purity of all final tested compounds was established to be >95% by reverse-phase HPLC on a Waters Breeze HPLC system with a SunFire C_{18} analytical column (4.6 mm × 150 mm, 5 μm) using acetonitrile−water (both containing 0.1% TFA) as the mobile phase (gradient: 30−100% acetonitrile, flow 1.5 mL/min), with UV monitoring at the fixed wavelength of 254 nm. Low-resolution mass spectra were obtained using an Agilent Technologies 6130 quadrupole LC/MS. HRMS data were obtained at the Mass Spectrometry Facility at Indiana University Chemistry Department (http://msf.chem.indiana.edu) on a Waters/Macromass LCT (electrospray ionization ESI).

Azide Synthesis. Commercially available amine/hydrazine (20 mmol) was dissolved in dry DMF (40 mL) under nitrogen. To this solution was added Et_3N (20 mmol) and acid chloride (20 mmol) via syringe at 0 °C under nitrogen. The mixture was stirred at 0 °C for 30 min and then at room temperature for another 2 h. Next, solid NaN_3 (30 mmol) was added and the reaction mixture was stirred overnight. The mixture was poured into water (100 mL) and extracted with EtOAc (3 × 100 mL). The combined extracts were washed with water (3 × 50 mL) and brine (50 mL). The organic layer was dried over Na_2SO_4, filtered, and evaporated under reduced pressure. Silica gel flash chromatography (10% ethyl acetate in hexanes) gave the desired azide product in 50−90% isolated yield.

Salicylic Acid Library Synthesis. To 2 mL vials were added 133 μL of core **1** (100 mM in THF), 167 μL of appropriate azide (100 mM in *t*-BuOH), 33 μL of TBTA (12 mM in DMF), 67 μL of $CuSO_4$ (10 mM in water), and 100 μL of sodium ascorbate (33.3 mM in water). Thus, the total volume of the reaction was 0.5 mL and the final concentration was 26.6 mM for core **1**, 32 mM for each azide, 0.798 mM for TBTA, 1.33 mM for $CuSO_4$, and 6.64 mM for sodium ascorbate. The vials were then capped and shaken at room temperature for 12 h. Subsequently, 1.0 mL DMSO was added to each vial, and the solutions were then transferred to 386-well plates for screening.

Methyl 4-Amino-2-hydroxybenzoate (2). Dimethyl sulfate (11.4 mL, 0.12 mol) was added to a mixture of 4-aminosalicylic acid (15.3 g, 0.1 mol), anhydrous sodium carbonate (12.96 g, 0.12 mol), and acetone (300 mL) at room temperature. After being stirred for 24 h at room temperature, the reaction mixture was filtered. Filtrate was concentrated under vacuum. The residue was purified by silica gel column chromatography to provide the product **2** (16.79 g, 86%).

Methyl 4-(Dimethylamino)-2-hydroxybenzoate (3). Paraformaldehyde (15.3 g, 0.51 mol) and $NaCNBH_3$ (16 g, 0.254 mol) were added portionwise to a solution of **2** (8.5 g, 50.8 mmol) in acetic acid (150 mL) at 0 °C, and the mixture was stirred at room temperature for 4 h. After evaporation, the residue was dissolved in ethyl acetate, washed with saturated $NaHCO_3$, brine, and dried over Na_2SO_4. After evaporation of solvent, the residue was purified by silica gel column chromatography to afford **3** (7.74 g, 78%). ^{1}H NMR (500 MHz, $CDCl_3$) δ 10.93 (s, 1H), 7.63 (d, J = 9.05 Hz, 1H), 6.19 (dd, J = 9.05, 2.5 Hz, 1H), 6.11 (d, J = 2.5 Hz, 1H), 3.86 (s, 3H), 2.99 (s, 6H); ^{13}C NMR (125 MHz, $CDCl_3$) δ 170.67, 163.27, 155.61, 131.01, 104.13, 100.82, 97.87, 51.53, 39.93. Mass calculated for $C_{10}H_{13}NO_3$ [M], 195, found $[M + H]^+$, 196.

Methyl 4-(Dimethylamino)-2-hydroxy-5-iodobenzoate (4). A solution of iodine (2.9 g, 11.4 mmol) in ether (15 mL) was added dropwise to a suspension of compound **3** (2.5 g, 12.8 mmol) and K_2CO_3 (2.6 g, 18.8 mmol) in water (15 mL) at room temperature over 2 h. The reaction mixture was then stirred at room temperature for an additional 30 min. Then, the reaction mixture was acidified to pH 3 with 2 N HCl and extracted with diethyl ether. The combined organic extractions were washed with brine, dried over Na_2SO_4, and concentrated in vacuo. Purification by flash chromatography (SiO_2) afforded compound **4** (1.73 g, 42%). ^{1}H NMR (500 MHz, $CDCl_3$) δ 10.73 (s, 1H), 8.22 (s, 1H), 6.55 (s, 1H), 3.91 (s, 3H), 2.84 (s, 6H); ^{13}C NMR (125 MHz, $CDCl_3$) δ 169.28, 162.82, 161.29, 141.68, 108.55, 108.11, 80.07, 52.24, 44.26. Mass calculated for $C_{10}H_{12}INO_3$ [M], 321, found $[M + H]^+$, 322.

Methyl 4-(Dimethylamino)-2-hydroxy-5-(phenylethynyl)benzoate (5). A mixture of methyl 4-(dimethylamino)-2-hydroxy-5-iodobenzoate **4** (6.5 g, 20.2 mmol), phenylacetylene (3.10 g, 30.4 mmol), bis(triphenylphosphine)palladium(II) chloride (0.288 g, 0.41 mmol), and CuI (0.155 g, 0.81 mmol) was loaded in a flask, which was degassed and backfilled with nitrogen. Then Et_3N (11.3 mL, 80.8 mmol) and solvent DMF were added. The resulting mixture was stirred under a nitrogen atmosphere at room temperature for 4 h. The reaction was monitored by TLC to ensure completion. After removal of solvent under reduced pressure, the residue was purified by column chromatography on silica gel to afford **5** (5.32 g, 89%). ^{1}H NMR (500 MHz, $CDCl_3$) δ 10.93 (s, 1H), 7.94 (s, 1H), 7.48 (m, 2H), 7.31 (m, 3H), 6.31 (s, 1H), 3.90 (s, 3H), 3.12 (s, 6H); ^{13}C NMR (125 MHz, $CDCl_3$) δ 169.95, 162.79, 159.36, 137.37, 131.03, 128.46, 127.96, 124.03, 104.45, 104.06, 103.02, 92.63, 88.88, 51.99, 42.66. Mass calculated for $C_{18}H_{17}NO_3$ [M], 295, found $[M + H]^+$, 296.

Methyl 6-Hydroxy-3-iodo-1-methyl-2-phenyl-1*H*-indole-5-carboxylate (6). To a solution of **5** (5.2 g, 17.6 mmol) in CH_2Cl_2 (100 mL) was added iodine (8.9 g, 35 mmol). After the resulting mixture was stirred at room temperature for an additional 4 h, 100 mL of CH_2Cl_2 was added, and the resulting mixture was washed with 10% aqueous NaS_2O_3 solution (3 × 50 mL), brine (50 mL), dried over Na_2SO_4, and concentrated in vacuo. Purification by flash chromatography afforded **6** (6.23 g, 87%). ^{1}H NMR (500 MHz, $CDCl_3$) δ 10.88 (s, 1H), 7.96 (s, 1H), 7.45 (m, 5H), 6.78 (s, 1H), 3.98 (s, 3H), 3.54 (s, 3H); ^{13}C NMR (125 MHz, $CDCl_3$) δ 171.29, 158.34, 142.88, 142.59, 131.22, 130.82, 129.06, 128.59, 124.30, 124.20, 107.64, 96.26, 59.53, 52.26, 32.23. Mass calculated for $C_{17}H_{14}INO_3$ [M], 407, found $[M + H]^+$, 408.

Methyl 6-Hydroxy-1-methyl-2-phenyl-3-((trimethylsilyl)ethynyl)-1*H*-indole-5-carboxylate (7). To a solution of **6** (6.52 g, 16.0 mmol), bis(triphenylphosphine)palladium(II) chloride (225 mg, 0.320 mmol), and CuI (122 mg, 0.640 mmol) in DMF were added (trimethylsilyl)acetylene (2.35 g, 24.01 mmol) and Et_3N (6.48 g, 64.04 mmol), and the reaction was stirred at room temperature under nitrogen for 4 h. The reaction was quenched with water, and the aqueous phase was extracted with ethylene chloride three times. The combined organic extract was dried over sodium sulfate, and the solvent was removed under vacuum. The residue was purified by silica gel column chromatography using 15:1 hexanes/ethyl acetate to provide compound **7** (4.4 g, 73%). ^{1}H NMR (500 MHz, $CDCl_3$) δ 10.91 (s, 1H), 8.23 (s, 1H), 7.60 (m, 2H), 7.48 (m, 3H), 6.83 (s, 1H), 4.00 (s, 3H), 3.64 (s, 3H), 0.21 (s, 9H); ^{13}C NMR (125 MHz, $CDCl_3$) δ 171.36, 158.23, 145.76, 141.86, 130.13, 129.99, 128.65, 122.68, 122.05, 107.57, 98.98, 97.91, 96.28, 52.13, 31.81, 0.14. Mass calculated for $C_{22}H_{23}NO_3Si$ [M], 377, found $[M + H]^+$, 378.

Methyl 3-Ethynyl-6-hydroxy-1-methyl-2-phenyl-1*H*-indole-5-carboxylate (8). To a solution of **7** (8.22 g, 21.77 mmol) in THF (100 mL) was added TBAF (6.86 g, 21.77 mmol). The solution was allowed to stir for 4 h before addition of 200 mL of methylene chloride to the reaction. The resulting solution was washed with water and brine and dried over sodium sulfate. The solvent was removed under vacuum. The residue was purified by silica gel column chromatography to provide compound **8** (4.58 g, 69%). ^{1}H NMR (500 MHz, $CDCl_3$) δ 10.90 (s, 1H), 8.24 (s, 1H), 7.60 (m, 2H), 7.51 (m, 2H), 6.82 (m, 1H), 3.98 (s, 1H), 3.19 (s, 1H), 3.17 (s, 1H); ^{13}C NMR (125 MHz, $CDCl_3$) δ 171.30, 158.24, 145.71, 141.73, 130.10, 129.96, 128.84, 128.52, 122.47, 122.34, 107.63, 96.59, 96.31, 80.05, 52.11, 31.64. Mass calculated for $C_{19}H_{15}NO_3$ [M], 305, found $[M + H]^+$, 306.

3-Ethynyl-6-hydroxy-1-methyl-2-phenyl-1*H*-indole-5-carboxylic Acid (1). Compound **8** (6.20 g, 20.31 mmol) was dissolved in 80 mL of THF, followed by the addition of a KOH solution (4.56 g, 81.24 mmol KOH in 80 mL of water). The mixture was refluxed for 2 h, cooled to room temperature, acidified to pH 3, and extracted with EtOAc three times. The organic layers were combined, washed with brine, dried over sodium sulfate, and concentrated in vacuum. This crude product was quickly taken to click reaction without purification. ^{1}H NMR (500 MHz, $CDCl_3$) δ 11.42 (s, 1H), 8.83 (s, 1H), 7.61 (m, 3H), 7.56 (m, 2H), 7.07 (s, 1H), 3.36 (s, 1H), 2.18 (s, 3H). Mass calculated for $C_{18}H_{13}NO_3$ [M], 291, found $[M + H]^+$, 292.

6-Hydroxy-1-methyl-3-(1-(3-oxo-3-(phenylamino)propyl)-1*H*-1,2,3-triazol-4yl)-2-phenyl-1*H*-indole-5-carboxylic Acid (14). A mixture of core **1** (50 mg, 0.172 mmol), 3-azido-*N*-phenylpropanamide (49 mg, 0.26 mmol), TBTA (2.7 mg, 0.005 mmol), $CuSO_4 \cdot 5H_2O$ (2.2 mg, 0.0088 mmol), sodium ascorbate (8.5 mg, 0.043 mmol) in THF (1 mL), *t*-BuOH (1 mL), and H_2O (1 mL) was stirred at room temperature under nitrogen for 24 h. The solvent was removed in vacuo. The resultant solid was then washed three times with water and purified by reversed-phase HPLC to yield the title compound as a white solid (33 mg, 40%). ^{1}H NMR (500 MHz, DMSO-d_6) δ 13.64 (s, 1H), 11.38 (s, 1H), 9.99 (s, 1H), 8.77 (s, 1H), 7.47 (m, 8H), 7.31 (t, J = 7.5 Hz, 2H), 7.27 (s, 1H), 7.05 (t, J = 7.5 Hz, 1H), 4.58 (t, J = 2.0 Hz, 2H), 3.48 (s, 3H), 2.89 (t, J = 2.0 Hz, 2H); ^{13}C NMR (125 MHz, DMSO-d_6) δ 173.05, 167.95, 157.35, 141.39, 138.87, 138.36, 130.60, 130.36, 129.06, 128.84, 128.66, 124.35, 123.25, 120.45, 119.24, 119.11, 107.10, 104.92, 99.49, 95.84, 45.39, 36.49, 30.79. HRMS (ESI) mass calculated for $C_{27}H_{24}N_5O_4$ $[M + H]^+$, 482.1828, found $[M + H]^+$, 482.1813.

3-(1-(2-(Biphenyl-4-ylamino)-2-oxoethyl)-1*H*-1,2,3-triazol-4-yl)-6-hydroxy-1-methyl-2-phenyl-1*H*-indole-5-carboxylic Acid (9a). A mixture of core **1** (50 mg, 0.172 mmol), 2-azido-*N*-(biphenyl-4-yl)acetamide (65 mg, 0.26 mmol), TBTA (2.7 mg, 0.005 mmol), $CuSO_4 \cdot 5H_2O$ (2.2 mg, 0.0088 mmol), sodium ascorbate (8.5 mg, 0.043 mmol) in THF (1 mL), *t*-BuOH (1 mL), and H_2O (1 mL) was stirred at room temperature under nitrogen for 24 h. The solvent was removed in vacuo. The resultant solid was then washed three times with water and purified by reversed-phase HPLC to yield the title compound as a white solid (31 mg, 33%). ^{1}H NMR (500 MHz, DMSO-d_6) δ 11.39 (s, 1H), 10.52 (s, 1H), 8.79 (s, 1H), 7.65 (m, 6H), 7.56 (m, 3H), 7.52 (m, 2H), 7.44 (t, J = 7.5 Hz, 2H), 7.41 (s, 1H), 7.33 (t, J = 7.5 Hz, 1H), 7.03 (s, 1H), 5.29 (s, 2H), 3.51 (s, 3H); ^{13}C NMR (125 MHz, DMSO-d_6) δ 141.94, 141.82, 140.02, 138.90, 138.33, 135.90, 131.25, 131.03, 129.67, 129.45, 129.40, 127.56, 126.73, 122.45, 120.09, 119.77, 105.40, 100.02, 52.65, 31.33. HRMS (ESI) mass calculated for $C_{32}H_{26}N_5O_4$ $[M + H]^+$, 544.1985, found $[M + H]^+$, 544.2001.

3-(1-(3-(Biphenyl-4-ylamino)-3-oxopropyl)-1*H*-1,2,3-triazol-4-yl)-6-hydroxy-1-methyl-2-phenyl-1*H*-indole-5-carboxylic Acid (9). A mixture of core **1** (50 mg, 0.172 mmol), 3-azido-*N*-(biphenyl-4-yl)propanamide (69 mg, 0.26 mmol), TBTA (2.7 mg, 0.005 mmol), $CuSO_4 \cdot 5H_2O$ (2.2 mg, 0.0088 mmol), sodium ascorbate (8.5 mg, 0.043 mmol) in THF (1 mL), *t*-BuOH (1 mL), and H_2O (1 mL) was stirred at room temperature under nitrogen for 24 h. The solvent was removed in vacuo. The resultant solid was then washed three times with water and purified by reversed-phase HPLC to yield the title compound as a white solid (42 mg, 44%). ^{1}H NMR (500 MHz, DMSO-d_6) δ 11.35 (s, 1H), 10.09 (s, 1H), 8.76 (s, 1H), 7.64 (m, 7H), 7.50−7.41 (m, 7H), 7.33 (m, 1H), 7.28 (s, 1H), 7.00 (s, 1H), 4.59 (t, J = 6.5 Hz, 2H), 3.47 (s, 3H), 2.90 (t, J = 6.5 Hz, 2H); ^{13}C NMR (125

MHz, DMSO-d_6) δ 173.08, 168.07, 157.38, 141.44, 141.42, 139.70, 138.42, 138.36, 134.97, 130.64, 130.41, 129.13, 128.89, 127.03, 126.90, 126.26, 124.36, 120.52, 119.52, 119.28, 107.13, 104.95, 99.53, 95.88, 45.44, 36.57, 30.83. HRMS (ESI): mass calculated for $C_{33}H_{28}N_5O_4$ $[M + H]^+$, 558.2141, found $[M + H]^+$, 558.2122.

3-(1-(4-(Biphenyl-4-ylamino)-4-oxobutyl)-1*H*-1,2,3-triazol-4-yl)-6-hydroxy-1-methyl-2-phenyl-1*H*-indole-5-carboxylic Acid (9b). A mixture of core **1** (50 mg, 0.172 mmol), 4-azido-*N*-(biphenyl-4-yl)butanamide (73 mg, 0.26 mmol), TBTA (2.7 mg, 0.005 mmol), $CuSO_4 \cdot 5H_2O$ (2.2 mg, 0.0088 mmol), sodium ascorbate (8.5 mg, 0.043 mmol) in THF (1 mL), *t*-BuOH (1 mL), and H_2O (1 mL) was stirred at room temperature under nitrogen for 24 h. The solvent was removed in vacuo. The resultant solid was then washed three times with water and purified on reversed phase HPLC to yield the desired title compound as a white solid (46 mg, 47%). ^{1}H NMR (500 MHz, DMSO-d_6) δ 11.38 (s, 1H), 10.01 (s, 1H), 8.77 (s, 1H), 7.63 (m, 6H), 7.53 (m, 3H), 7.50 (m, 2H), 7.44 (t, J = 7.5 Hz, 2H), 7.33 (t, J = 7.5 Hz, 1H), 7.31 (s, 1H), 7.03 (s, 1H), 4.36 (t, J = 7.0 Hz, 2H), 3.52 (s, 3H), 2.31 (t, J = 7.0 Hz, 2H), 2.06 (t, J = 7.0 Hz, 2H); ^{13}C NMR (125 MHz, DMSO-d_6) δ 173.53, 170.61, 157.84, 141.94, 140.17, 139.09, 138.94, 135.18, 131.13, 130.99, 129.59, 129.36, 127.45, 127.31, 126.67, 124.80, 120.86, 119.91, 119.80, 107.60, 105.53, 99.99, 96.36, 49.20, 33.23, 31.33, 29.60. HRMS (ESI): mass calculated for $C_{34}H_{30}N_5O_4$ $[M + H]^+$, 572.2298, found $[M + H]^+$, 572.2274.

SHP2 Cloning, Expression, and Purification. A PCR-based strategy was used to amplify the sequence coding for the catalytic domain of SHP2 (residues 262−528) from the full length construct. The PCR products were gel purified, digested with *Nde* I and *Xho* I restriction enzymes (Invitrogen), and ligated to the linearized pET-21a(+) vector (Novagen). The ligation products were used to transform *E. coli* BL21(DE3) plys competent cells (Novagen). Gene sequence was confirmed by DNA sequencing carried out by the DNA Sequencing Facility at Indiana University School of Medicine. For protein expression, transformed *E. coli* cells were grown at 37 °C in Luria broth (LB) containing 100 μg/mL ampicillin for 4 h to an absorbance of 0.6 at 600 nm and then induced for protein production with 0.4 mM IPTG overnight at 20 °C. Cells were harvested by centrifugation (6500 rpm for 15 min at 4 °C), and the cell pellets from 1 L LB medium were suspended in 30 mL of ice-cold lysis buffer consisting of 5 mM imidazole, 500 mM NaCl, 20 mM Tris-HCl (pH 7.9), 0.05 mg/mL trypsin inhibitor, and 0.1 mM PMSF. The suspensions were passed twice through a French press at 1200 psi, and the cell lysates were centrifuged at 4 °C for 45 min at 16 000 rpm. The supernatants were mixed with 2 mL of Ni-NTA Agarose (His*Bind resin) (Qiagen) at 4 °C for 50 min, washed with 200 mL of binding buffer (5 mM imidazole, 500 mM NaCl, 20 mM Tris-HCl (pH 7.9)), followed by 20 mL of washing buffer (20 mM imidazole, 500 mM NaCl, 20 mM Tris-HCl (pH 7.9)), and then eluted with 20 mL of elution buffer (200 mM imidazole, 500 mM NaCl, 20 mM Tris-HCl (pH 7.9)). The elute was dialyzed for 6 h at 4 °C against 1 L of buffer A (100 mM NaCl, 20 mM MES (pH 6.0), 1 mM EDTA), and then loaded onto a Mono S column equilibrated at 4 °C with buffer A. The column was washed with 10 mL of buffer A and then eluted with a 40 mL linear gradient of 0 to 1 M NaCl in buffer A. SHP2 was eluted at 0.35 M NaCl. The column fractions were analyzed by measuring the absorbance at 280 nm and by carrying out SDS−PAGE analysis. The fractions were combined, dialyzed against 1 L of buffer A, concentrated at 4 °C to 7 mg/mL using an Amicon concentrator, and then stored at −80 °C. The SHP2 protein was shown to be homogeneous by SDS−PAGE analysis.

Kinetic Analysis of SHP2 Inhibition by the Salicylic Acid Based Library. The phosphatase activity of SHP2 was assayed using *p*-nitrophenyl phosphate (*p*NPP) as a substrate at 25 °C in 50 mM 3,3-dimethylglutarate buffer, pH 7.0, containing 1 mM EDTA with an ionic strength of 0.15 M adjusted by NaCl. The salicylic acid based library was screened in a 96-well format at 10 μM compound concentration. The reaction was initiated by the addition of 5 μL of the enzyme to 195 μL of reaction mixture containing 10 μM test compound and various concentrations of *p*NPP and quenched after 5 min by the addition of 50 μL of 5 N NaOH. The nonenzymatic hydrolysis of *p*NPP was corrected by measuring the control without the addition of enzyme. The amount of product *p*-nitrophenol was determined from the absorbance at 405 nm detected by a Spectra MAX340 microplate spectrophotometer (Molecular Devices) using a molar extinction coefficient of 18 000 M^{-1} cm^{-1}.

Compounds exhibiting more than 50% of inhibitory activity against SHP2 were selected for IC_{50} measurement. The reaction was started by the addition of 5 μL of the enzyme to 195 μL of reaction mixture containing 2.9 mM (the K_m value) of *p*NPP and various concentrations of the inhibitor. The reaction was quenched after 5 min by the addition of 50 μL of 5 N NaOH, and then 200 μL of reaction mixture was transferred to a 96-well plate. The absorbance at 405 nm was detected by a Spectra MAX340 microplate spectrophotometer (Molecular Devices). IC_{50} values were calculated by fitting the absorbance at 405 nm versus inhibitor concentration to the following equation:

$$A_I/A_0 = IC_{50}/(IC_{50} + [I])$$

where A_I is the absorbance at 405 nm of the sample in the presence of inhibitor, A_0 is the absorbance at 405 nm in the absence of inhibitor, and [I] is the concentration of the inhibitor.

For selectivity studies, the PTPs, including PTP1B, SHP1, FAP1, Lyp, HePTP, VHR, LMWPTP, Cdc14, LAR, PTPα, and CD45, were expressed and purified from *E. coli*. The inhibition assay for these PTPs were performed under the same conditions as SHP2 except using a different *p*NPP concentration corresponding to the K_m of the PTP studied. Inhibitor concentrations used for IC_{50} measurements cover the range from 0.2× to 5× of the IC_{50} value.

To evaluate potential nonspecific promiscuous inhibition, we first determine whether the compound displays time-dependence inhibition by measuring the IC_{50} values with and without enzyme preincubation with the inhibitor. We also determine the effect of bovine serum albumin (0.1 mg/mL) on IC_{50} values. Finally, we also assess whether the IC_{50} values can be influenced by the presence of detergents such as 0.1% of Triton X-100. A well-behaved classical and reversible active site directed inhibitor should not exhibit any dependence on time, BSA, and detergents.

***K*$_i$ Measurement.** The SHP2-catalyzed hydrolysis of *p*NPP in the presence of **9** was assayed at 25 °C and in the assay buffer described above. The mode of inhibition and K_i value were determined in the following manner. At various fixed concentrations of inhibitor (0−3 K_i), the initial rate at a series of *p*NPP concentrations was measured by following the production of *p*-nitrophenol as describe above, ranging from 0.2- to 5-fold the apparent K_m values. The data were fitted to appropriate equations using SigmaPlot-Enzyme Kinetics to obtain the inhibition constant and to assess the mode of inhibition.

Retroviral Vectors and Retroviral Transduction. The wild-type SHP2 cDNA was mutated at nucleotides 226 (G > A) or 181 (G > T) using QuikChange site-directed mutagenesis kit (Stratagene, La Jolla, CA) to yield amino acid changes E76K or D61Y, respectively.[45] Each cDNA was subcloned into the murine stem cell virus (MSCV)-based bicistronic retroviral vector, pMIEG3, in tandem with enhanced green fluorescent protein (EGFP). Ecotropic retroviral supernatants (pMIEG3-wild-type SHP2, pMIEG3-SHP2/E76K, and pMIEG3-SHP2/D61Y) were prepared using Eco-Phoenix packaging cells. Bone marrow low density mononuclear cells from C57Bl/6 mice (Jackson Laboratories, Bar Harbor, ME) were purified using a Ficoll gradient. Cells were prestimulated at a concentration of 2×10^6 cells/mL in IMDM, 20% fetal calf serum (Hyclone,

Logan, UT), 2 mM glutamine, 1% penicillin/streptomycin, stem cell factor (SCF), granulocyte-colony stimulating factor (G-CSF), and thrombopoietin (Tpo) all at 100 ng/mL (growth factors from Peprotech, Rocky Hill, NJ) for 24 h. Cells were then transferred to retroviral supernatant on plates coated with fibronectin fragments (Retronectin, Takara, Madison, WI) with SCF, G-CSF, and Tpo 100 ng/mL for an additional 48 h. Transduced cells were collected using fluorescence activated cell sorting (FACS) for EGFP positive cells.

[^{3}H]Thymidine Incorporation. Proliferation was assessed by conducting thymidine incorporation assays on EGFP-sorted wild-type SHP2-, SHP2/D61Y-, or SHP2/E76K-expressing hematopoietic progenitors. Briefly, cells were washed and starved in 0.2% BSA with or without any growth factors for 4 h. Then 5×10^4 cells were cultured in 96-well plates in various concentrations of granulocyte-macrophage colony-stimulating factor (GM-CSF) in the absence or presence of **9**. Cells were cultured for 16 h and subsequently pulsed with 1.0 μCi of [^{3}H]thymidine for 6−8 h. Cells were harvested using an automated 96-well cell harvester (Brandel, Gaithersburg, MD), and thymidine incorporation was determined as counts per minute (CPM).

Cell Culture and Immunoblot Analysis. HEK293 cells were cultured in Dulbecco modified Eagle medium (DMEM) with 10% fetal calf serum. Then 4×10^5 cells were plated into each well of 12-well plates and cultured for 24 h. For biochemical studies, cells were serum-deprived for 16 h followed by treatment with vehicle, **9**, or **14** for 3 h. The cells were then stimulated with epidermal growth factor (EGF, 2 ng/mL) for the indicated time followed by preparation of total cell protein lysates. Lysates (30 μg) were electrophoresed on a 10% polyacrylamide gel, transferred to a nitrocellulose membrane, and probed with antiphospho-ERK1/2 and anti-ERK1/2 (Cell Signaling Technology, Beverly, MA).

Crystallization of SHP2 with 9 and X-ray Data Collection. All crystallization experiments were carried out at room temperature using the hanging drop vapor diffusion method. For cocrystallization, 100 μL of SHP2 stock (7.0 mg/mL) in 20 mM Tris-HCL (pH 7.5), 50 mM NaCl, 0.1 mM EDTA, and 3.0 mM DTT was mixed with 1 μL of compound **9** stock solution (50 mM in DMSO). Crystals of SHP2·**9** complex were obtained at room temperature by vapor diffusion in hanging drops. Protein drops were equilibrated against a reservoir solution containing 20% w/v polyethylene glycol 3350, 200 mM magnesium acetate tetrahydrate, and 100 mM HEPES buffer (pH 7.7). The space group of the crystals is $P2_1$ (Table 3). For X-ray data collection, the crystals were transferred into 5 μL of cryoprotectant buffer containing 30% w/v polyethylene glycol 3350, 100 mM NaCl, and 100 mM HEPES (pH 7.7) and were allowed to soak for 30 min. The crystals were then flash-cooled by liquid nitrogen. X-ray data were collected at 23 ID beamline at APS (Argonne, IL). Data were processed using the program HKL2000,[51] and the statistics are provided in Table 3.

Structural Determination and Refinement. The structure of SHP2·**9** was solved by molecular replacement using the program AMoRe.[52] The structure of SHP2 (PDB entry code 3B7O),[46] without the solvent molecules and the first 16 residues, was used as a search model. The resulting difference Fourier map indicated some alternative tracing, which was incorporated into the model. The map revealed the density for the bound **9** in the active site of SHP2. The structure was refined to 2.0 Å resolution with the program CNS,[53] first using simulated annealing at 2500 K and then alternating positional and individual temperature factor refinement cycles. The progress of the refinement was evaluated by the improvement in the quality of the electron density maps, and the reduced values of the conventional R factor ($R = \sum_h ||F_o| - |F_c|| / \sum_h |F_o|$) and the free R factor (3.8% of the reflections omitted from the refinement).[54] Electron density maps were inspected, and the model was modified on an interactive graphics workstation with the program O.[55] Finally, water molecules were added gradually as the refinement progressed. They were assigned in the $|F_o| - |F_c|$ difference Fourier maps with a 3σ cutoff level for inclusion in the model.

Acknowledgment. This work was supported by National Institutes of Health Grants CA69202, CA126937, and HL82981 and the Clarian Values Fund for Research (Grant VFR-245). X.Z. was also supported in part by the State Scholarship Fund from China Scholarship Council, and S.C.N. was supported by the National Institutes of Health (Grant F31AG031648).

Supporting Information Available: Figure showing the inhibition curves used to determine the IC_{50} values for compounds listed in Table 4. This material is available free of charge via the Internet at http://pubs.acs.org.

References

(1) Hunter, T. The Croonian lecture 1997. The phosphorylation of proteins on tyrosine: its role in cell growth and disease. *Philos. Trans. R. Soc. London, Ser. B* **1998**, *353*, 583–605.
(2) Tonks, N. K.; Neel, B. G. Combinatorial control of the specificity of protein tyrosine phosphatases. *Curr. Opin. Cell Biol.* **2001**, *13*, 182–195.
(3) Zhang, Z.-Y. Protein tyrosine phosphatases: prospects for therapeutics. *Curr. Opin. Chem. Biol.* **2001**, *5*, 416–423.
(4) Ventura, J. J.; Nebreda, A. R. Protein kinases and phosphatases as therapeutic targets in cancer. *Clin. Transl. Oncol.* **2006**, *8*, 153–160.
(5) Krause, D. S.; Van Etten, R. A. Tyrosine kinases as targets for cancer therapy. *N. Engl. J. Med.* **2005**, *353*, 172–187.
(6) Neel, B. G.; Gu, H.; Pao, L. The "Shp" ing news: SH2 domain-containing tyrosine phosphatases in cell signaling. *Trends Biochem. Sci.* **2003**, *28*, 284–293.
(7) Chan, R. J.; Feng, G. S. PTPN11 is the first identified proto-oncogene that encodes a tyrosine phosphatase. *Blood* **2007**, *109*, 862–867.
(8) Tiganis, T.; Bennett, A. M. Protein tyrosine phosphatase function: the substrate perspective. *Biochem. J.* **2007**, *402*, 1–15.
(9) Tartaglia, M.; Mehler, E. L.; Goldberg, R.; Zampino, G.; Brunner, H. G.; Kremer, H.; van der Burgt, I.; Crosby, A. H.; Ion, A.; Jeffery, S.; Kalidas, K.; Patton, M. A.; Kucherlapati, R. S.; Gelb, B. D. Mutations in PTPN11, encoding the protein tyrosine phosphatase SHP-2, cause Noonan syndrome. *Nat. Genet.* **2001**, *29*, 465–468.
(10) Tartaglia, M.; Gelb, B. D. Noonan syndrome and related disorders: genetics and pathogenesis. *Annu. Rev. Genomics Hum. Genet.* **2005**, *6*, 45–68.
(11) Tartaglia, M.; Niemeyer, C. M.; Fragale, A.; Song, X.; Buechner, J.; Jung, A.; Hahlen, K.; Hasle, H.; Licht, J. D.; Gelb, B. D. Somatic mutations in PTPN11 in juvenile myelomonocytic leukemia, myelodysplastic syndromes and acute myeloid leukemia. *Nat. Genet.* **2003**, *34*, 148–150.
(12) Tartaglia, M.; Martinelli, S.; Cazzaniga, G.; Cordeddu, V.; Iavarone, I.; Spinelli, M.; Palmi, C.; Carta, C.; Pession, A.; Arico, M.; Masera, G.; Basso, G.; Sorcini, M.; Gelb, B. D.; Biondi, A. Genetic evidence for lineage-related and differentiation stage-related contribution of somatic PTPN11 mutations to leukemogenesis in childhood acute leukemia. *Blood* **2004**, *104*, 307–313.
(13) Loh, M. L.; Vattikuti, S.; Schubbert, S.; Reynolds, M. G.; Carlson, E.; Lieuw, K. H.; Cheng, J. W.; Lee, C. M.; Stokoe, D.; Bonifas, J. M.; Curtiss, N. P.; Gotlib, J.; Meshinchi, S.; Le Beau, M. M.; Emanuel, P. D.; Shannon, K. M. Mutations in PTPN11 implicate the SHP-2 phosphatase in leukemogenesis. *Blood* **2004**, *103*, 2325–2331.
(14) Loh, M. L.; Reynolds, M. G.; Vattikuti, S.; Gerbing, R. B.; Alonzo, T. A.; Carlson, E.; Cheng, J. W.; Lee, C. M.; Lange, B. J.; Meshinchi, S. Children's Cancer Group. PTPN11 mutations in pediatric patients with acute myeloid leukemia: results from the Children's Cancer Group. *Leukemia* **2004**, *18*, 1831–1834.
(15) Kratz, C. P.; Niemeyer, C. M.; Castleberry, R. P.; Cetin, M.; Bergsträsser, E.; Emanuel, P. D.; Hasle, H.; Kardos, G.; Klein, C.; Kojima, S.; Stary, J.; Trebo, M.; Zecca, M.; Gelb, B. D.; Tartaglia., M.; Loh., M. L. The mutational spectrum of PTPN11 in juvenile myelomonocytic leukemia and Noonan syndrome/myeloproliferative disease. *Blood* **2005**, *106*, 2183–2185.
(16) Bentires-Alj, M.; Paez, J. G.; David, F. S.; Keilhack, H.; Halmos, B.; Naoki, K.; Maris, J. M.; Richardson, A.; Bardelli, A.; Sugarbaker, D. J.; Richards, W. G.; Du, J.; Girard, L.; Minna, J.

D.; Loh, M. L.; Fisher, D. E.; Velculescu, V. E.; Vogelstein, B.; Meyerson, M.; Sellers, W. R.; Neel, B. G. Activating mutations of the Noonan syndrome-associated SHP2/PTPN11 gene in human solid tumors and adult acute myelogenous leukemia. *Cancer Res.* **2004**, *64*, 8816–8820.
(17) Chan, G.; Kalaitzidis, D.; Neel, B. G. The tyrosine phosphatase Shp2 (*PTPN11*) in cancer. *Cancer Metastasis Rev.* **2008**, *27*, 179–192.
(18) Miyamoto, D.; Miyamoto, M.; Takahashi, A.; Yomogita, Y.; Higashi, H.; Kondo, S.; Hatakeyama, M. Isolation of a distinct class of gain-of-function SHP-2 mutants with oncogenic RAS-like transforming activity from solid tumors. *Oncogene* **2008**, *27*, 3508–3515.
(19) Hatakeyama, M. Oncogenic mechanisms of the *Helicobacter pylori* CagA protein. *Nat. Rev. Cancer* **2004**, *4*, 688–694.
(20) Stommel, J. M.; Kimmelman, A. C.; Ying, H.; Nabioullin, R.; Ponugoti, A. H.; Wiedemeyer, R.; Stegh, A. H.; Bradner, J. E.; Ligon, K. L.; Brennan, C.; Chin, L.; DePinho, R. A. Coactivation of receptor tyrosine kinases affects the response of tumor cells to targeted therapies. *Science* **2007**, *318*, 287–290.
(21) Chen, L.; Sung, S. S.; Yip, M. L.; Lawrence, H. R.; Ren, Y.; Guida, W. C.; Sebti, S. M.; Lawrence, N. J.; Wu, J. Discovery of a novel shp2 protein tyrosine phosphatase inhibitor. *Mol. Pharmacol.* **2006**, *70*, 562–570.
(22) Lawrence, H. R.; Pireddu, R.; Chen, L.; Luo, Y.; Sung, S. S.; Szymanski, A. M.; Yip, M. L.; Guida, W. C.; Sebti, S. M.; Wu, J.; Lawrence, N. J. Inhibitors of Src homology-2 domain containing protein tyrosine phosphatase-2 (Shp2) based on oxindole scaffolds. *J. Med. Chem.* **2008**, *51*, 4948–4956.
(23) Hellmuth, K.; Grosskopf, S.; Lum, C. T.; Würtele, M.; Röder, N.; von Kries, J. P.; Rosario, M.; Rademann, J.; Birchmeier, W. Specific inhibitors of the protein tyrosine phosphatase Shp2 identified by high-throughput docking. *Proc. Natl. Acad. Sci. U.S.A.* **2008**, *105*, 7275–7280.
(24) Yu, W. M.; Guvench, O.; Mackerell, A. D.; Qu, C. K. Identification of small molecular weight inhibitors of Src homology 2 domain-containing tyrosine phosphatase 2 (SHP-2) via in silico database screening combined with experimental assay. *J. Med. Chem.* **2008**, *51*, 7396–7404.
(25) Wu, D.; Pang, Y.; Ke, Y.; Yu, J.; He, Z.; Tautz, L.; Mustelin, T.; Ding, S.; Huang, Z.; Feng, G.-S. A conserved mechanism for control of human and mouse embryonic stem cell pluripotency and differentiation by shp2 tyrosine phosphatase. *PLoS One* **2009**, *4*, e4914.
(26) Zhang, Z.-Y. Protein tyrosine phosphatases: structure and function, substrate specificity, and inhibitor development. *Annu. Rev. Pharmacol. Toxicol.* **2002**, *42*, 209–234.
(27) Puius, Y. A.; Zhao, Y.; Sullivan, M.; Lawrence, D. S.; Almo, S. C.; Zhang, Z.-Y. Identification of a second aryl phosphate-binding site in protein-tyrosine phosphatase 1B: a paradigm for inhibitor design. *Proc. Natl. Acad. Sci. U.S.A.* **1997**, *94*, 13420–13425.
(28) Zhang, S.; Zhang, Z.-Y. PTP1B as a drug target: recent development in PTP1B inhibitor discovery. *Drug Discovery Today* **2007**, *12*, 373–381.
(29) Sarmiento, M.; Wu, L.; Keng, Y.-F.; Song, L.; Luo, Z.; Huang, Z.; Wu, G.-Z.; Yuan, A. K.; Zhang, Z.-Y. Structure-based discovery of small molecule inhibitors targeted to protein tyrosine phosphatase 1B. *J. Med. Chem.* **2000**, *43*, 146–155.
(30) Liang, F.; Huang, Z.; Lee, S.-Y.; Liang, J.; Ivanov, M. I.; Alonso, A.; Bliska, J. B.; Lawrence, D. S.; Mustelin, T.; Zhang, Z.-Y. Aurintricarboxylic acid blocks in vitro and in vivo activity of YopH, an essential virulent factor of *Yersinia pestis*, the agent of plague. *J. Biol. Chem.* **2003**, *278*, 41734–41741.
(31) Horton, D. A.; Bourne, G. T.; Smythe, M. L. The combinatorial synthesis of bicyclic privileged structures or privileged substructures. *Chem. Rev.* **2003**, *103*, 893–930.
(32) Gul, W.; Hamann, M. T. Indole alkaloid marine natural products: an established source of cancer drug leads with considerable promise for the control of parasitic, neurological and other diseases. *Life Sci.* **2005**, *78*, 442–453.
(33) Kolb, H. C.; Finn, M. G.; Sharpless, K. B. Click chemistry: diverse chemical function from a few good reactions. *Angew. Chem., Int. Ed.* **2001**, *40*, 2004–2021.
(34) Lewis, W. G.; Green, L. G.; Grynszpan, F.; Radić, Z.; Carlier, P. R.; Taylor, P.; Finn, M. G.; Sharpless, K. B. Click chemistry in situ: acetylcholinesterase as a reaction vessel for the selective assembly of a femtomolar inhibitor from an array of building blocks. *Angew. Chem., Int. Ed.* **2002**, *41*, 1053–1057.
(35) Lee, L. V.; Mitchell, M. L.; Huang, S. J.; Fokin, V. V.; Sharpless, K. B.; Wong, C. H. A potent and highly selective inhibitor of human alpha-1,3-fucosyltransferase via click chemistry. *J. Am. Chem. Soc.* **2003**, *125*, 9588–9589.
(36) Manetsch, R.; Krasiński, A.; Radić, Z.; Raushel, J.; Taylor, P.; Sharpless, K. B.; Kolb, H. C. In situ click chemistry: enzyme inhibitors made to their own specifications. *J. Am. Chem. Soc.* **2004**, *126*, 12809–12818.
(37) Srinivasan, R.; Uttamchandani, M.; Yao, S. Q. Rapid assembly and in situ screening of bidentate inhibitors of protein tyrosine phosphatases. *Org. Lett.* **2006**, *8*, 713–716.
(38) Xie, J.; Seto, C. T. A two stage click-based library of protein tyrosine phosphatase inhibitors. *Bioorg. Med. Chem.* **2007**, *15*, 458–473.
(39) Yu, X.; Sun, J.-P.; He, Y.; Guo, X.-L.; Liu, S.; Zhou, B.; Hudmon, A.; Zhang, Z.-Y. Structure, inhibitor, and regulatory mechanism of Lyp, a lymphoid-specific tyrosine phosphatase implicated in autoimmune diseases. *Proc. Natl. Acad. Sci. U.S.A.* **2007**, *104*, 19767–19772.
(40) Deb, T. B.; Wong, L.; Salomon, D. S.; Zhou, G.; Dixon, J. E.; Gutkind, J. S.; Thompson, S. A.; Johnson, G. R. A common requirement for the catalytic activity and both SH2 domains of SHP-2 in mitogen-activated protein (MAP) kinase activation by the ErbB family of receptors. A specific role for SHP-2 in map, but not c-Jun amino-terminal kinase activation. *J. Biol. Chem.* **1998**, *273*, 16643–16646.
(41) Qu, C. K.; Yu, W. M.; Azzarelli, B.; Feng, G. S. Genetic evidence that Shp-2 tyrosine phosphatase is a signal enhancer of the epidermal growth factor receptor in mammals. *Proc. Natl. Acad. Sci. U.S.A.* **1999**, *96*, 8528–8533.
(42) Maroun, C. R.; Naujokas, M. A.; Holgado-Madruga, M.; Wong, A. J.; Park, M. The tyrosine phosphatase SHP-2 is required for sustained activation of extracellular signal-regulated kinase and epithelial morphogenesis downstream from the met receptor tyrosine kinase. *Mol. Cell. Biol.* **2000**, *20*, 8513–8525.
(43) Egan, S. E.; Giddings, B. W.; Brooks, M. W.; Buday, L.; Sizeland, A. M.; Weinberg, R. A. Association of Sos Ras exchange protein with Grb2 is implicated in tyrosine kinase signal transduction and transformation. *Nature* **1993**, *363*, 45–51.
(44) Emanuel, P. D.; Bates, L. J.; Castleberry, R. P.; Gualtieri, R. J.; Zuckerman, K. S. Selective hypersensitivity to granulocyte-macrophage colony-stimulating factor by juvenile chronic myeloid leukemia hematopoietic progenitors. *Blood* **1991**, *77*, 925–929.
(45) Chan, R. J.; Leedy, M. B.; Munugalavadla, V.; Voorhorst, C. S.; Li, Y.; Yu, M.; Kapur, R. Human somatic PTPN11 mutations induce hematopoietic-cell hypersensitivity to granulocyte-macrophage colony-stimulating factor. *Blood* **2005**, *105*, 3737–3742.
(46) Barr, A. J.; Ugochukwu, E.; Lee, W. H.; King, O. N.; Filippakopoulos, P.; Alfano, I.; Savitsky, P.; Burgess-Brown, N. A.; Muller, S.; Knapp, S. Large-scale structural analysis of the classical human protein tyrosine phosphatome. *Cell* **2009**, *136*, 352–363.
(47) Zhang, Z.-Y. Mechanistic studies on protein tyrosine phosphatases. *Prog. Nucleic Acid Res. Mol. Biol.* **2003**, *73*, 171–220.
(48) Jia, Z.; Barford, D.; Flint, A. J.; Tonks, N. K. Structural basis for phosphotyrosine peptide recognition by protein tyrosine phosphatase 1B. *Science* **1995**, *268*, 1754–1758.
(49) Sun, J.-P.; Fedorov, A. A.; Lee, S.-Y.; Guo, X.-L.; Shen, K.; Lawrence, D. S.; Almo, S. C.; Zhang, Z.-Y. Crystal structure of PTP1B in complex with a potent and selective bidentate inhibitor. *J. Biol. Chem.* **2003**, *278*, 12406–12414.
(50) Yang, J.; Cheng, Z.; Niu, T.; Liang, X.; Zhao, Z. J.; Zhou, G. W. Structural basis for substrate specificity of protein-tyrosine phosphatase SHP-1. *J. Biol. Chem.* **2000**, *275*, 4066–4071.
(51) Otwinowski, Z.; Minow, W. Processing of X-ray diffraction data collected in oscillation mode. *Methods Enzymol.* **1997**, *276*, 307–326.
(52) Navaza, J. AMoRe: an automated package for molecular replacement. *Acta Crystallogr. A* **1994**, *50*, 157–163.
(53) Brünger, A. T.; Adams, P. D.; Clore, G. M.; DeLano, W. L.; Gros, P.; Grosse-Kunstleve, R. W.; Jiang, J. S.; Kuszewski, J.; Nilges, M.; Pannu, N. S.; Read, R. J.; Rice, L. M.; Simonson, T.; Warren, G. L. Crystallography & NMR system: a new software suite for macromolecular structure determination. *Acta Crystallogr. D* **1998**, *54*, 905–921.
(54) Brünger, A. T. The free *R* value: a novel statistical quantity for assessing the accuracy of crystal structures. *Nature* **1992**, *355*, 472–475.
(55) Jones, T. A.; Zou, J. Y.; Cowan, S. W.; Kjeldgaard, G. J. Improved methods for building protein models in electron density maps and the location of errors in these models. *Acta Crystallogr. A.* **1991**, *47*, 110–119.